

Tropical plumes and extreme precipitation in subtropical and tropical West Africa

By PETER KNIPPERTZ* and JONATHAN E. MARTIN

Department of Atmospheric and Oceanic Sciences, University of Wisconsin–Madison, Madison, Wisconsin, USA

(Received 8 October 2004; revised 25 April 2005)

SUMMARY

Three cases of extreme precipitation in October, January and March/April over subtropical north-western and tropical West Africa have been selected in order to study the moisture transports, precipitation generation mechanisms and large-scale dynamics involved. All cases show strong tropical–extratropical interactions and elongated cloud bands extending from the Tropics into the subtropics, usually referred to as tropical plumes (TPs). Investigations are based on observational data and high-resolution output from simulations using the University of Wisconsin–Nonhydrostatic Modeling System. Trajectory analyses show that moisture is transported from the tropical easterly mid-level flow, the monsoonal southerlies and the north-easterly trade winds to provide precipitable water and potential instability at mid-tropospheric levels. The instability is released through ascent related both to weak quasi-geostrophic forcing to the east of an upper-level trough and to the strong, inertially unstable and highly divergent upper-level subtropical jet (STJ) accompanying the TP. In the January and March cases the passage of a precursor upper-level trough over the same location precedes the development and initiates the moisture transport from the deep Tropics. The associated north-westerly cold advection supports the generation of precipitation by triggering convection over the tropical Atlantic Ocean, whose outflow feeds into the STJ over Africa, and by enhancing the vertical mass transport within the intertropical discontinuity over and near West Africa. In October, when the still active African monsoon facilitates the extraction of tropical moisture, a wave in the tropical easterlies and strong trade winds from the southern hemisphere are dominant factors. Low-level cyclogenesis and frontogenesis only play roles in the late stages of the developments. The elongated, mostly positively tilted potential-vorticity (PV) streamers associated with the observed troughs form as a result of an equatorward transport of high-PV air downstream of a large ridge over the North Atlantic. The rapid amplification of the ridge is achieved through a combination of negative horizontal PV advection and diabatic reduction of upper-level PV through latent heating within a cloud band that forms in connection with an explosive baroclinic development near the east coast of North America.

KEYWORDS: Explosive cyclogenesis Inertial instability Potential instability Potential vorticity Subtropical jet Trajectories

1. INTRODUCTION

This study deals with three extended cool season events of unusual heavy precipitation in the area from the northern margin of the West African Tropics to the subtropical Atlas mountain chain in north-western Africa (see Fig. 1). Apart from the fairly wet tropical zone (12–16°N) affected by the African monsoon during boreal summer, most of the region receives annual rainfalls of well below 300 mm, and even below 100 mm in the Sahara (20–29°N; see Fig. 8 in Griffiths and Soliman (1972) and Fig. 1 in Nicholson (2001)) where rainfalls are sporadic all the year round. During 1978–98 Ouarzazate (see Table 1 for details of all stations used) in southern Morocco, for example, received half of its average annual precipitation of 117 mm during only 3–4 days. This is, to some extent, a consequence of the manner in which the Atlas Mountains act as a barrier to the propagation of cool season synoptic systems from the Atlantic Ocean (Knippertz *et al.* 2003a).

According to Fig. 14 in Griffiths and Soliman (1972) significant rainfall events are even less frequent in the Sahara. Examining these rare events is thus an essential contribution to the understanding of the local climate.

* Corresponding author, present affiliation: Institute for Physics of the Atmosphere, University of Mainz, Germany. e-mail: knippertz@uni-mainz.de

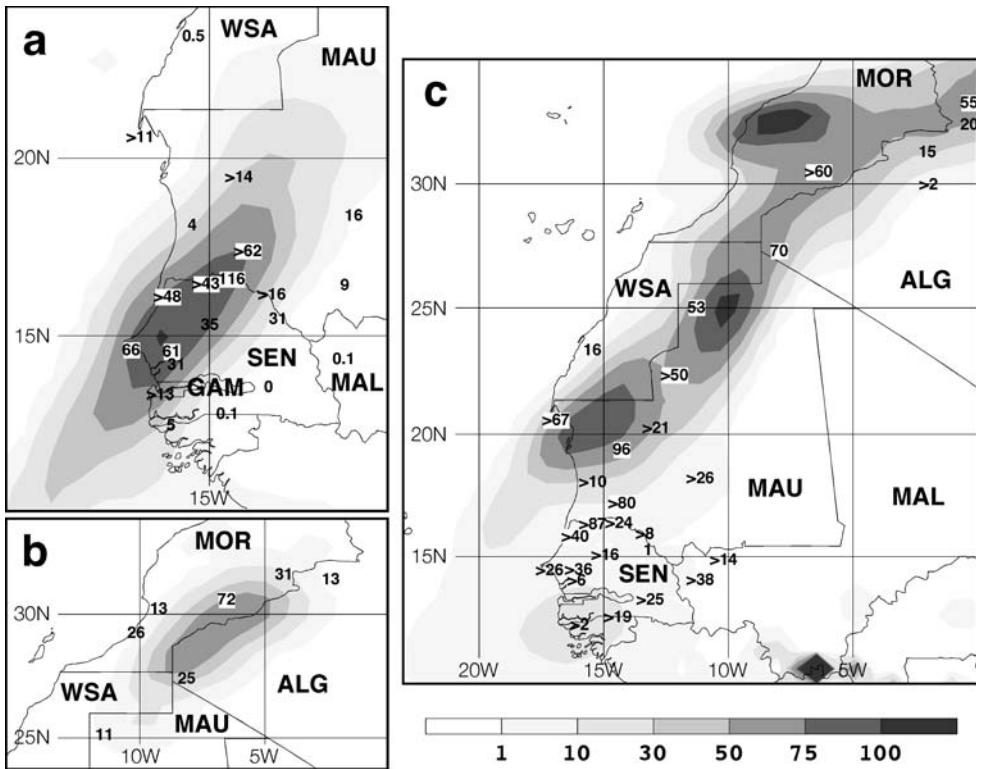


Figure 1. Accumulated precipitation (mm) from the University of Wisconsin–Nonhydrostatic Modeling System simulations (shaded, see key) and from station observations (black numbers; see Table 1) for: (a) case I, from 06 UTC 9 to 06 UTC 11 January 2002; (b) case II, from 18 UTC 30 March to 00 UTC 2 April 2002; and (c) case III, from 18 UTC 20 to 06 UTC 24 October 2003. Stations with missing data during the precipitation period have ‘>’ preceding the precipitation sum (see section 2); ‘0’ represents a trace of precipitation. Abbreviations for countries are given in Table 1.

The first of three cases of unusually heavy precipitation under investigation (hereafter cases I, II and III) affected north-western Senegal and south-western Mauritania in the middle of the local dry season in January 2002. Such off-season rainfalls are sometimes referred to as Heug or Mango rains. The event was classified as the most intense January event on record, and produced dramatic socio-economic impacts through widespread flooding, destruction of infrastructure, large losses of livestock, harvest and seeds, as well as casualties due to the collapse of houses and hypothermia. Case II occurred in the springtime of 2002 and affected southern Morocco, western Algeria and northern Mauritania, with some locations receiving more than half their annual precipitation from this event. As documented by Fink and Knippertz (2003, hereafter FK03) the event caused detrimental flash floods, but also refilled local water reservoirs. Case III in autumn 2003 affected the entire region from northern Senegal to the west Algerian Atlas Mountains, and brought more than the annual average precipitation totals to some arid, sparsely populated Saharan sites. The event contributed significantly to favourable breeding conditions for desert locusts, leading to a devastating outbreak in large parts of (north-) West Africa in the following months (FAO 2004).

In this paper we show that all three of these precipitation cases result from a particular type of tropical–extratropical interaction that involves the equatorward penetration of subtropical upper-level troughs, strong subtropical jet (STJ) streaks, elongated

TABLE 1. SYNOPTIC STATIONS IN NORTH-WEST AND WEST AFRICA AND PRECIPITATION (mm) DURING THREE CASES OF HEAVY RAINFALL

WMO Station number	Name	Country ¹	Latitude (°N)	Longitude (°W)	Elevation ² (m)	Accumulated precipitation ³ (mm)		
						Case I	Case II	Case III
60060	Sidi Ifni	MOR	29.22	10.11	66		26	
60096	Villa Cisneros	WSA	23.42	15.52	12	0.5		16
60210	Er-Rachidia	MOR	31.56	4.24	1042		31	
60252	Agadir Al Massira	MOR	30.20	9.25	74		13	
60265	Ouarzazate	MOR	30.56	6.54	1140		72	>60
60549	Mecheria	ALG	33.32	0.15	1149			55
60560	Ain Sefra	ALG	32.46	0.36	1059			20
60571	Bechar Ouakda	ALG	31.37	2.14	816		13	15
60602	Beni Abbes	ALG	30.08	2.10	505			>2
60656	Tindouf	ALG	27.40	8.08	439		25	70
61235	Yelimane	MAL	15.07	10.34	100			>14
61257	Kayes	MAL	14.26	11.26	47	0.1		>38
61401	Bir Moghrein	MAU	25.14	11.37	360		11	53
61404	Zouerate	MAU	22.45	12.29	343			>50
61415	Nouadhibou	MAU	20.56	17.02	3	>11		>67
61421	Atar	MAU	20.31	13.04	224			>21
61437	Akjoujt	MAU	19.45	14.22	120	>14		96
61442	Nouakchott	MAU	18.06	15.57	3	4		>10
61450	Tidjikja	MAU	18.34	11.26	402	16		>26
61461	Boutilimit	MAU	17.32	14.41	75	>62		>80
61489	Rosso	MAU	16.30	15.49	6	>43		>87
61492	Kaedi	MAU	16.09	13.31	18	>16		>8
61498	Kiffa	MAU	16.38	11.24	115	9		
61600	Saint Louis	SEN	16.03	16.27	4	>48		>40
61612	Podor	SEN	16.39	14.58	7	116		>24
61627	Linguere	SEN	15.23	15.07	21	35		>16
61630	Matam Ouro Sogui	SEN	15.39	13.15	17	31		1
61641	Dakar Yoff	SEN	14.44	17.30	24	66		>26
61666	Diourbel	SEN	14.39	16.14	9	61		>36
61679	Kaolack	SEN	14.08	16.04	7	31		>6
61687	Tambacounda	SEN	13.46	13.41	50	0		>25
61695	Ziguinchor	SEN	12.33	16.16	23	5		>2
61698	Kolda	SEN	12.53	14.58	10	0.1		>9
61701	Banjul	GAM	13.21	16.48	33	>13		

¹ Abbreviations for countries are as follows: ALG, Algeria; GAM, Gambia; MOR, Morocco; MAL, Mali; MAU, Mauritania; SEN, Senegal; and WSA, Western Sahara.

² Above mean sea level.

³ Values marked by '>' are where only a lower bound for the accumulated precipitation can be given.

cloud bands on their equatorward side (termed tropical plumes (TPs, McGuirk *et al.* 1988)) and low-level trade wind surges (Kiladis and Weickmann 1992; Kiladis 1998). The study focuses on the evolution of precipitation (section 3), TPs and upper-level STJ streaks (section 4), moisture transports (section 5) and the mechanisms that generate the ascent in the precipitation regions (section 6). These latter include investigations of mid-level quasi-geostrophic (QG) forcing, inertial stability of the upper jet, frontogenetic and cyclogenetic processes, and the vertical stability of the involved air masses. Prior studies on the relation between TPs or TP-like events and cool season precipitation in the subtropics have not addressed most of these processes in detail (e.g. Dayan and Abramski 1983; Wright 1997; Ziv 2001; FK03). A common issue affecting synoptic and climatological studies on sparsely populated regions in West Africa is the lack of dense and high-quality observational data. For this reason the analyses in sections 3–6 make use of simulations by the University of Wisconsin–Nonhydrostatic Modeling System (UW-NMS), providing estimates of areal distributions of precipitation as well as

high-resolution dynamical variables and trajectories. A short description of the model is presented in section 2, together with an overview of the data and computational methods employed. In section 7 we address the large-scale upstream evolution that fosters the penetration of the involved upper-level troughs to low latitudes. The paper concludes with a summary and a discussion of the main results in section 8.

2. DATA

For all three precipitation events synoptic observations distributed by the World Meteorological Organization (WMO) are used, as detailed in Table 1. For comparisons with long-term averages we use the 1961–90 climatological normals (CLINOs, WMO 1996) of the respective stations. Unfortunately several reports are missing or questionable during the considered periods, some perhaps as a direct result of the heavy precipitation; therefore, alternative sources of information are considered. For case I we obtained daily precipitation totals for Senegal from a website of the Senegalese government (http://www.gouv.sn/meteo/cart_pluies.html). Additional conclusions on the upper and lower limits of the event totals can be drawn from the monthly numbers of rain days and accumulated precipitation amounts given in the *Monthly climatic data for the world* published by the National Climatic Data Center, Ashville, USA. Since uncertainties remain for some stations, only a lower bound for the accumulated precipitation can be given (see Table 1 and Fig. 1). For cases II and III the German research project IMPETUS* provided half-hourly precipitation data from stations along a north–south height transect from the Moroccan High Atlas to the fringe of the Sahara (see FK03). Satellite estimates of rainfall were obtained from the Global Precipitation Climatology Project (GPCP). The Space Science and Engineering Center of the University of Wisconsin in Madison provided twice-daily Meteosat images.

All three events were simulated using the UW-NMS (Tripoli 1992) operating on a single grid of 160×97 points with 75 km grid spacing spanning 15°S – 50°N , 84°W – 24°E . The model has 40 vertical levels up to 22.6 km. Each simulation was run for 8.5 days starting several days before the respective precipitation event. For model initialization and updates at the boundaries, twice daily (00 and 12 UTC) European Centre for Medium-Range Weather Forecasts (ECMWF) Tropical Ocean and Global Analysis data are used with $2.5^{\circ} \times 2.5^{\circ}$ grid spacing on standard pressure levels (Trenberth 1992). The goal of these simulations is to produce a physically consistent ‘interpolation’ of the ECMWF analyses. More details on the model configuration including the employed convective parametrization can be found in Mecikalski and Tripoli (2003). Trajectories were calculated from the hourly model data using the visualization software VIS5D (Hibbard *et al.* 1996). Knippertz (2005, hereafter KN05) used the same model output for a detailed study of the TP involved in case II.

3. PRECIPITATION

(a) Case I

According both to model results and to observations, precipitation begins around midday 9 January 2002 over Senegal and Gambia. The rainfall quickly intensifies, spreads into Mauritania and reaches its maximum intensity 24 h later. At this time the precipitation zone oriented south-west to north-east has a maximum extension of about

* Integratives Management Projekt für einen effizienten und tragfähigen Umgang mit Süßwasser in Westafrika (An integrated approach to the efficient management of scarce water resources in West Africa); see FK03 and www.impetus.uni-koeln.de.

1500 km. After remaining nearly stationary for another 24 h, the rain finally ceases around midday 11 January.

Figure 1(a) shows accumulated precipitation totals for the 48 h period 06 UTC 9 to 06 UTC 11 January 2002 from observations (numbers) and the model (shading). Maximum precipitation of 116 mm is observed at Podor near the Senegalese–Mauritanian border, corresponding to 54% of the annual CLINO value. At least three other stations in north-western Senegal and south-western Mauritania record rainfalls of more than 60 mm. The large variation in precipitation totals suggests mesoscale convective structures within the rain zone. Towards eastern Senegal and western Mali rainfall amounts sharply decrease. Towards the north the precipitation zone stretches into arid Mauritania and Western Sahara with moderate rainfalls of between 0.5 and 16 mm. CLINO January averages are nowhere higher than 2 mm throughout the affected area, revealing the extraordinary nature of this event. GPCP satellite estimates confirm the unusual rainfalls but with slightly smaller peak values.

The model produces a smooth precipitation zone with little structure at small-scales (Fig. 1(a)). Contributions from subgrid-scale convective precipitation are very small. The maximum grid point value of 104 mm is of the same magnitude as the observational maximum, but its location is displaced to the south-west. Overall observed and model-produced values are satisfyingly similar with only the large east–west extension of the precipitation band over Mauritania not fully reproduced. The model simulates an extension of the precipitation zone over the Atlantic Ocean, where no synoptic observations are available for comparison.

(b) *Case II*

Precipitation during case II is confined to the subtropical end of the investigation region. According both to model results and to observations, precipitation starts over the hyper-arid north-western Sahara in northern Mauritania during the day on 30 March 2002 and moves north-eastward towards the southern foothills of the High Atlas in southern Morocco. Heaviest rainfalls occur late on 31 March and during the first half of 1 April. The rain stops around 15 UTC 1 April. This corresponds with data from the IMPETUS stations (see Fig. 5 of FK03).

Figure 1(b) shows model and observation precipitation totals for the 54 h period 18 UTC 30 March to 00 UTC 2 April. The 72 mm recorded at Ouarzazate corresponds to 65% of the annual CLINO value. Unusual precipitation amounts of 11–31 mm are also observed at the arid stations of Bir Moghreïn, Tindouf, Er-Rachidia and Bechar. The precipitation is faithfully reproduced by the model, with a maximum grid point value of 69 mm near the Morocco–Algeria border. This is surprising given the presumably rain-enhancing steep orography of the Atlas region, which is not fully accounted for in the model. GPCP satellite estimates confirm the magnitude of the rainfalls, but place the maximum slightly to the north-west with respect to the model simulation.

(c) *Case III*

Case III affects the entire region from tropical Senegal to the subtropical Algerian Atlas Mountains. Both observations and model results reveal that rains start in Senegal and southern Mali in the course of the afternoon of 20 October 2003 and quickly spread into Mauritania by the next morning. Around 00 UTC 22 October the precipitation zone extends from Senegal into southern Morocco, and then further on towards the northern side of the Moroccan Atlas Mountains. No station observations are available for Senegal on 22 October, but the model results suggest that the southern end of the precipitation

zone moves quickly northward during the course of this day. From 12 UTC 22 to 00 UTC 24 October the precipitation also affects the Algerian Atlas region. For 23 October the model simulates heavy precipitation over the Moroccan Atlantic coast, well separated from the rest of the rain band.

Figure 1(c) shows accumulated precipitation for the 3.5-day period 18 UTC 20 to 06 UTC 24 October. At the southern end of the precipitation band observations range from a trace to over 80 mm. Occurring at the tail end of the local rainy season (see Fig. 5 of Camberlin and Diop (2003)), some event totals are substantially higher than climatological values for the entire month of October (16–38 mm in northern Senegal, see WMO (1996)). The extreme small-scale variations suggest the existence of cellular convection in this region. The model reproduces this quite unsatisfactorily; it simulates a broad region of moderate rainfalls, with maximum grid point precipitation of only 20 mm over southern Senegal and very little contribution from subgrid-scale convection. Tropical convection is a general weakness of most numerical models at the employed resolution.

Further to the north the model produces a second maximum of 96 mm over north-western Mauritania, which exactly matches the observation at Akjoujt to the south-east and agrees with GPCP satellite estimates. The grid point maximum of 107 mm over northern Mauritania is hard to validate due to the lack of nearby stations. However, the 70 mm in Tindouf, of which 46 mm falls in only 6 h, and the 53 mm in Bir Moghrein, are on the order of 1–1.5 times the long-term annual average and clearly underline the very unusual nature of this event. GPCP data reveal a slightly weaker maximum a little closer to the coast. Further to the north-east the model simulates precipitation above 50 mm along the southern foothills of the Atlas chain throughout southern Morocco and into western Algeria, which agrees with the observations at Ouarzazate and Mecheria. High-resolution measurements from the IMPETUS stations show event totals of 46–69 mm, rain intensities of up to $5 \text{ mm (30 min)}^{-1}$ and snow accumulations of up to 50 cm on the summits of the High Atlas. Most precipitation falls during the period 20 UTC 21 to 23 UTC 22 October. Over the Moroccan Atlantic coast the model produces another maximum of 122 mm. No station reports are available for this period, but an October total of 113 mm, or 3.6 times the long-term average, at Casablanca (33.34°N , 7.4°W) supports the occurrence of an unusual synoptic situation during this month. Overall model-simulated and observed precipitation amounts and distributions are gratifyingly similar.

4. TPS AND STJ STREAKS

(a) *Case 1*

Figure 2 shows Meteosat infrared (IR) images with superimposed UW-NMS streamlines and isotachs at the 345 K isentropic level, which is a typical level for convective outflow and the core of the STJ (see KN05). At 00 UTC 8 January some patchy clouds are observed to the east of the axis of a deep upper-level trough over the subtropical eastern Atlantic Ocean (Fig. 2(a)). The north-westerly flow in the eastern portion of the upstream ridge and the south-westerly flow out of the convectively active region over South America and the tropical Atlantic form the confluent entrance region of the moderate westerly STJ, with a maximum wind speed of 53 m s^{-1} over the Cape Verde Islands.

At 00 UTC 9 January, a few hours before the first rainfalls in West Africa, the circulation has not changed substantially, but the trough now reaches farther into the Tropics, and first indications of a downstream ridge over North Africa are evident

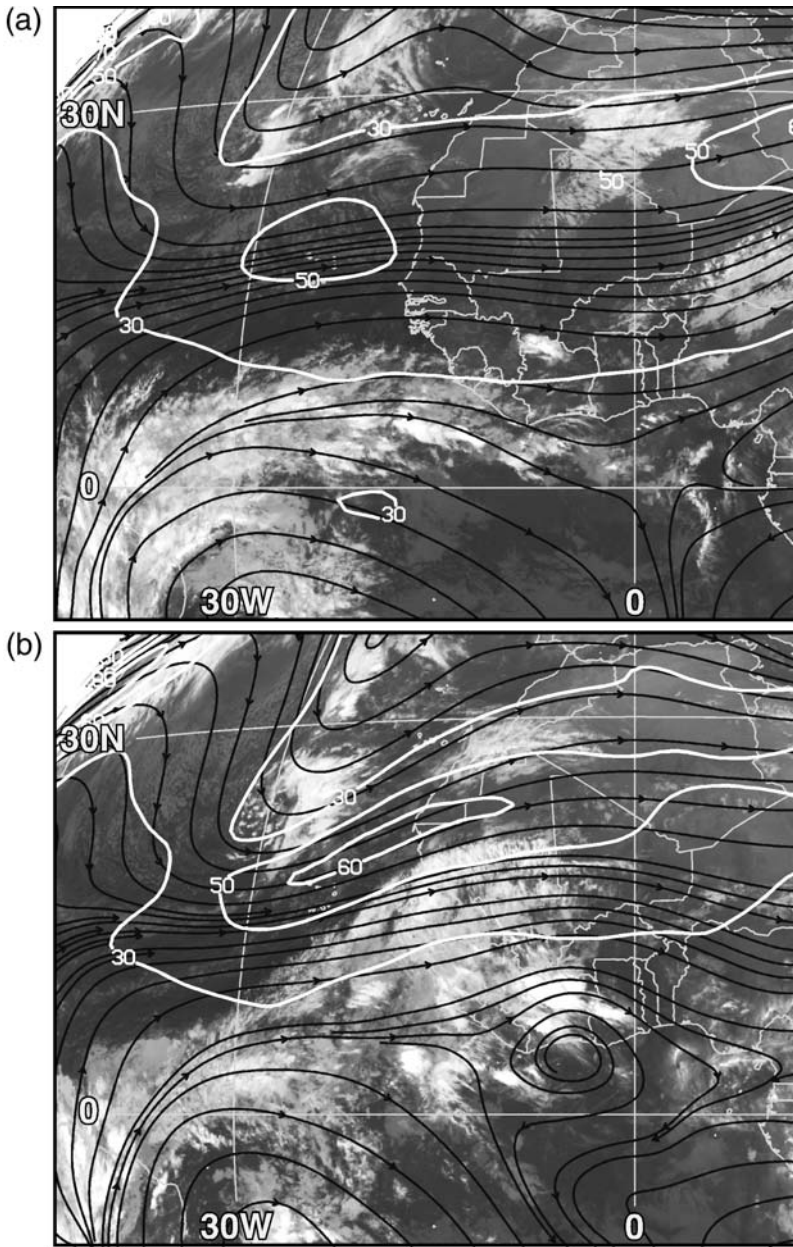


Figure 2. Meteosat IR satellite images during case I, with superimposed isotachs at the 345 K isentropic level in white (m s^{-1}) and streamlines in black for: (a) 00 UTC 8 January, (b) 00 UTC 9 January, and (c) 00 UTC 10 January 2002.

(Fig. 2(b)). The jet has tilted, intensified to 61 m s^{-1} and moved north-eastward to about 20°N , 20°W . The cloud mass at the southern tip of the trough shows the typical comma structure of a subtropical cyclone (e.g. Ramage 1962) with cellular convection behind it. In the Tropics, clouds have spread far into West Africa along the equatorward side of the jet. Strong convection and an anticyclonic circulation at upper-levels are evident over Ivory Coast (near 6°W) and the nearby Atlantic Ocean.

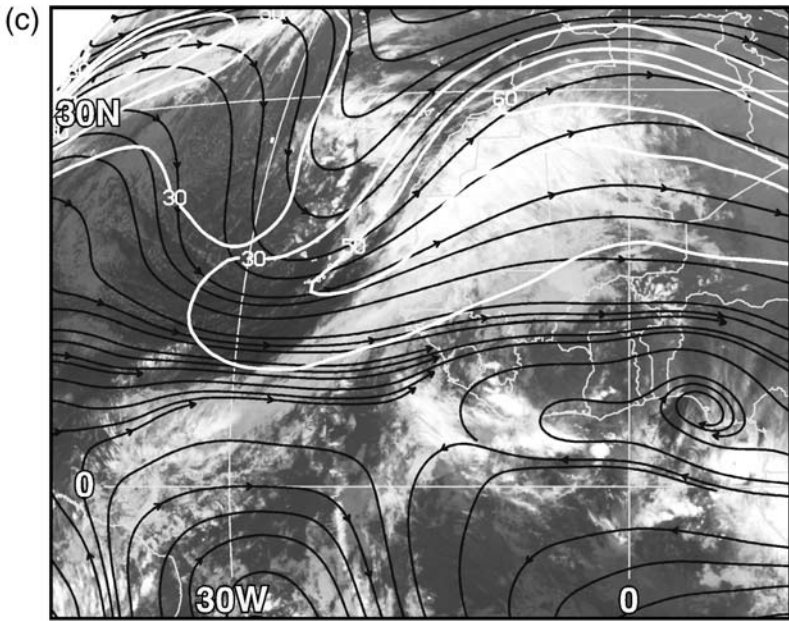


Figure 2. Continued.

Over the following 12 h the jet maximum remains stationary, but then quickly passes the amplifying ridge over North Africa, reaching its highest value of 68 m s^{-1} over the Algerian–Libyan border at 00 UTC 10 January (Fig. 2(c)). In the meantime a massive TP has formed that reaches from the equatorial Atlantic into the Algerian Sahara. Heavy precipitation occurs under its central portion over West Africa (see subsection 3(a)). Ongoing strong convection is observed to the south of the TP, leading to precipitation totals of up to 95 mm at stations in south-western West Africa (not shown). Note the clear separation between the intensified subtropical cyclone on the poleward side of the STJ and the sharp western edge of the TP aligned along the jet axis. Over the following 36 h the TP and jet quickly weaken (not shown).

(b) Case II

Since KN05 described the evolution during case II in detail, it is only summarized here. Compared to case I, the TP and STJ show a much slower evolution and a more pronounced south-west to north-east orientation in the early stages. The STJ propagates north-eastwards across the Atlantic Ocean, and steadily accelerates over a period of 5 days from 34 to nearly 80 m s^{-1} at 00 UTC 31 March. The TP forms during the last 36 h of this acceleration phase, and rainfall begins when the TP and the jet maximum reach north-west Africa. Figure 3 shows the mature TP and the 345 K jet maximum of 71 m s^{-1} at 00 UTC 1 April, when precipitation is heaviest over southern Morocco (see subsection 3(b)). The jet is in good agreement with ECMWF wind analyses (Fig. 2(f) in KN05). As in case I, strong convection is evident in the deep Tropics over West Africa to the south of the TP. Additionally, we note the clear indication of a subtropical cyclone close to the axis of the upper-trough on the poleward side of the jet, though the separation between the two cloud features is less distinct than in Fig. 2(c).

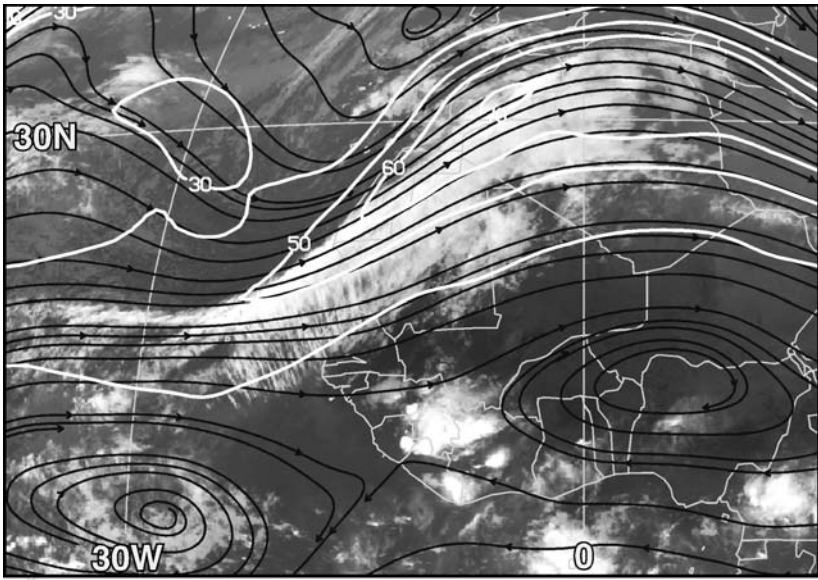


Figure 3. As Fig. 2 but for case II, 00 UTC 1 April 2002.

(c) Case III

At 12 UTC 20 October, shortly before precipitation starts over Senegal and Mali (see subsection 3(c)), a high-amplitude wave is located over the subtropical Atlantic Ocean (Fig. 4(a)). Some clouds are observed to the east of the axis of the trough, which is oriented south-west to north-east; these clouds extend to around 25°N , 30°W . Over West Africa and the adjacent tropical Atlantic widespread scattered clouds and convection are evident from the IR image, and streamlines depict strong divergent outflow (near 7°N , 21°W and 6°N , 13°W). The STJ oriented south-west to north-east reaches a maximum 345 K wind speed of only 37 m s^{-1} over the coast of Mauritania.

When the trough approaches West Africa, convection intensifies, a TP forms, and the wind speed maximum moves to southern Spain and increases to 73 m s^{-1} by 00 UTC 22 October (Fig. 4(b)). Heavy precipitation is observed in the Atlas region under the central portion of the TP (subsection 3(c)). A huge anticyclonic circulation over West Africa is evident in the streamlines. On 23 October the upper-trough begins to weaken, the TP breaks apart, and the jet core moves over the western Mediterranean Sea and decelerates (not shown).

5. MOISTURE TRANSPORT

(a) Case I

In order to trace back the sources of moisture for the record-breaking rains over West Africa, we computed numerous trajectories from the UW-NMS output. Figure 5 shows the tracks of three example trajectories, together with their height, mixing ratio (MR) and potential temperature, θ , for 4–11 January.

Trajectory 1 originates in the easterly low-level flow (height $\sim 2\text{ km}$) over tropical Africa and remains near the 310 K isentropic surface until 9 January (Figs. 5(a) and (d)). Around 00 UTC 6 January the parcel turns eastward over the Atlantic Ocean and later northward into southern Mauritania, while slowly ascending to 3.25 km. Throughout

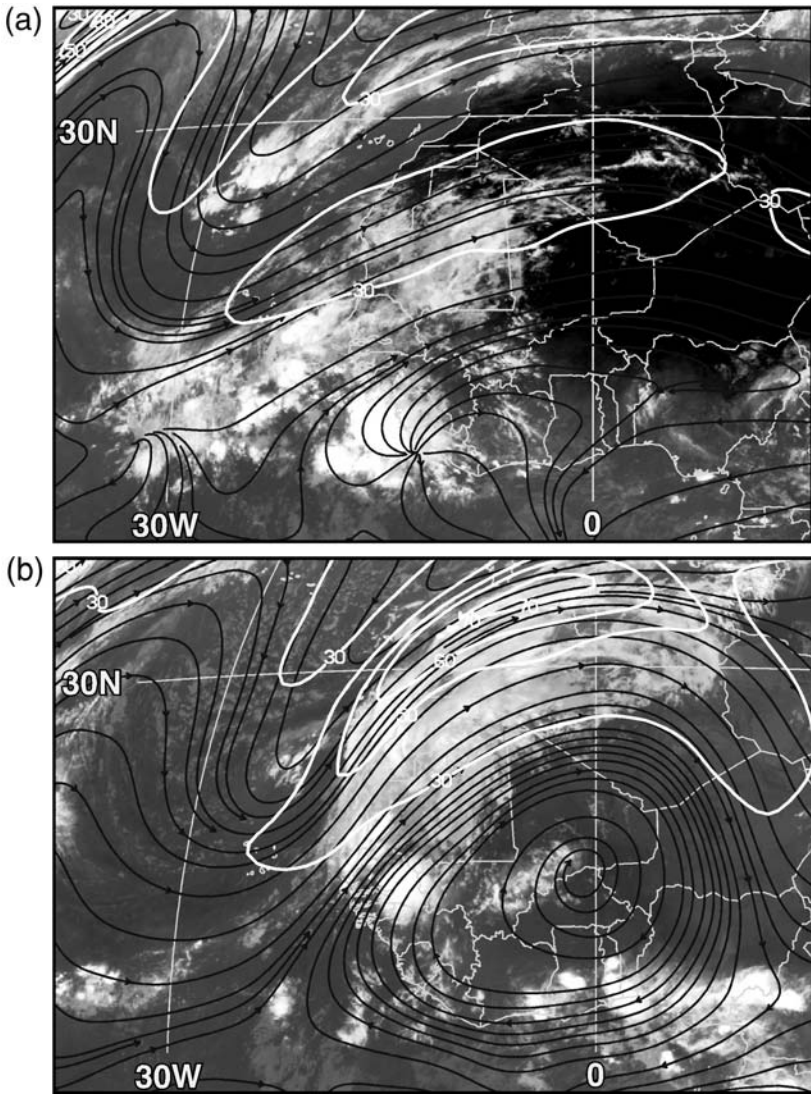


Figure 4. As Fig. 2 but for case III: (a) 12 UTC 20 October, and (b) 00 UTC 22 October 2003.

this period a MR of $\sim 6 \text{ g kg}^{-1}$ is maintained. Between 12 UTC 9 and 12 UTC 10 January the parcel rises to 9.4 km and quickly accelerates towards the STJ over western Algeria (Fig. 2(c)), feeding nearly all its moisture into the precipitation zone over Mauritania. The increase in θ of 23 K reflects the associated latent-heat release and convective mixing with hot Saharan air.

Trajectory 2 originates in the dry north-easterly trade winds over the Sahara (Figs. 5(b) and (e)). Initially the parcel remains in the lowest 1 km of the atmosphere, stays close to the 300 K isentropic surface and increases its MR to well above 10 g kg^{-1} over the tropical Atlantic. Between 00 UTC 7 and 00 UTC 9 January the parcel turns eastward and then northward, rises to 2.8 km, warms to 310 K and dries to 8 g kg^{-1} , suggesting its likely involvement in shallow convection. In the following 36 h the parcel

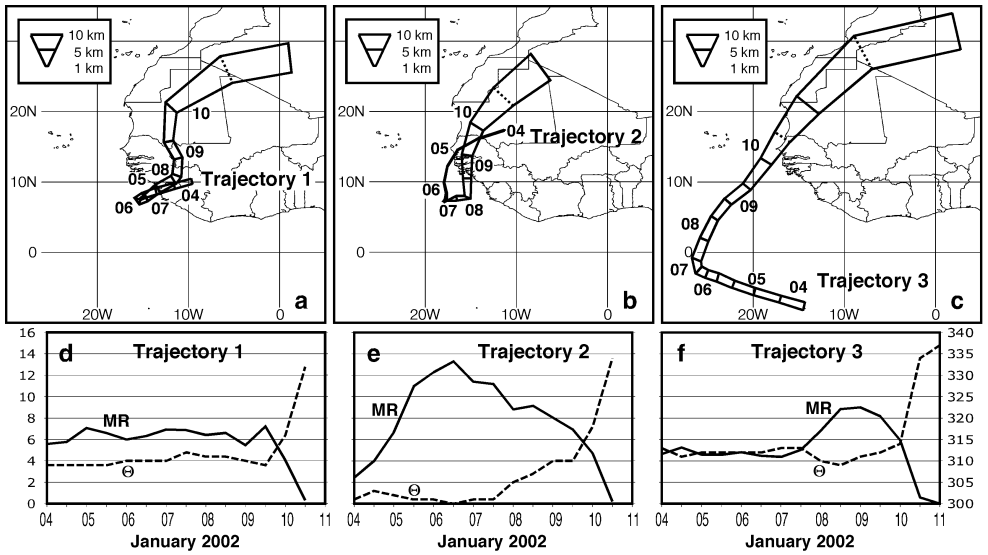


Figure 5. Three trajectories calculated from the University of Wisconsin–Nonhydrostatic Modeling System simulations for case I, all beginning at 00 UTC 4 January 2002: (a), (b) and (c) show the tracks with the width indicating the height (see key) every 12 h (marked by full lines across the track) or, later on, every 6 h (dashed lines across); numbers give the position at the start of each calendar day in January along the trajectories. Lower frames (d), (e) and (f), respectively, show the mixing ratio (MR, g kg^{-1} , left ordinate) and potential temperature (θ , K, right ordinate).

rises to 10.2 km and accelerates into western Algeria, dropping its moisture over the rain zone in Mauritania and warming through latent-heat release.

Trajectory 3 starts in the tropical easterlies at around 7.7°S (Figs. 5(c) and (f)). Remaining at heights around 3 km and maintaining a θ of ~ 312 K and a MR of ~ 4.8 g kg^{-1} , the parcel slowly progresses north-westward and reaches its westernmost point at 26.2°W at 12 UTC 7 January. In the following 36 h the parcel moves north-eastward and moistens to 9 g kg^{-1} , presumably in association with the convection in this region (see Figs. 2(a) and (b)). After 00 UTC 10 January the parcel quickly rises to over 10 km, while warming and drying in a similar manner to trajectories 1 and 2.

The previous analysis reveals that at around 12 UTC 7 January a substantial disturbance of the tropical circulation occurs that forces the trajectories to leave their westward and equatorward tracks toward the equatorial trough. Figures 6(a) and (b) show streamlines, isobars and convergence at 300 and 310 K, respectively, together with the positions of the trajectories from Fig. 5 at this time. At both levels a distinct cyclonic circulation is evident over the coast of Western Sahara. The downward northerly flow at 300 K to its west is indicative of a trade (wind) surge, and is associated with enhanced low-level convergence in the intertropical convergence zone over the Atlantic Ocean (Fig. 6(a)). The convergence triggers convection that eventually feeds its outflow into the STJ over Africa (Fig. 2). The downward crossing of pressure contours by the streamlines at both levels and the backing of the winds with height in Fig. 6 indicate subsidence and cold advection. The convergence of the trade surge with flow from the southern hemisphere (SH) just off the coast of West Africa triggers the lifting of trajectory 2. At 310 K parcels accelerate towards the low-pressure system in the subtropics, and then curve anticyclonically under the increasing Coriolis force and flow up the sloping isentropic surface towards North Africa (Fig. 6(b)).

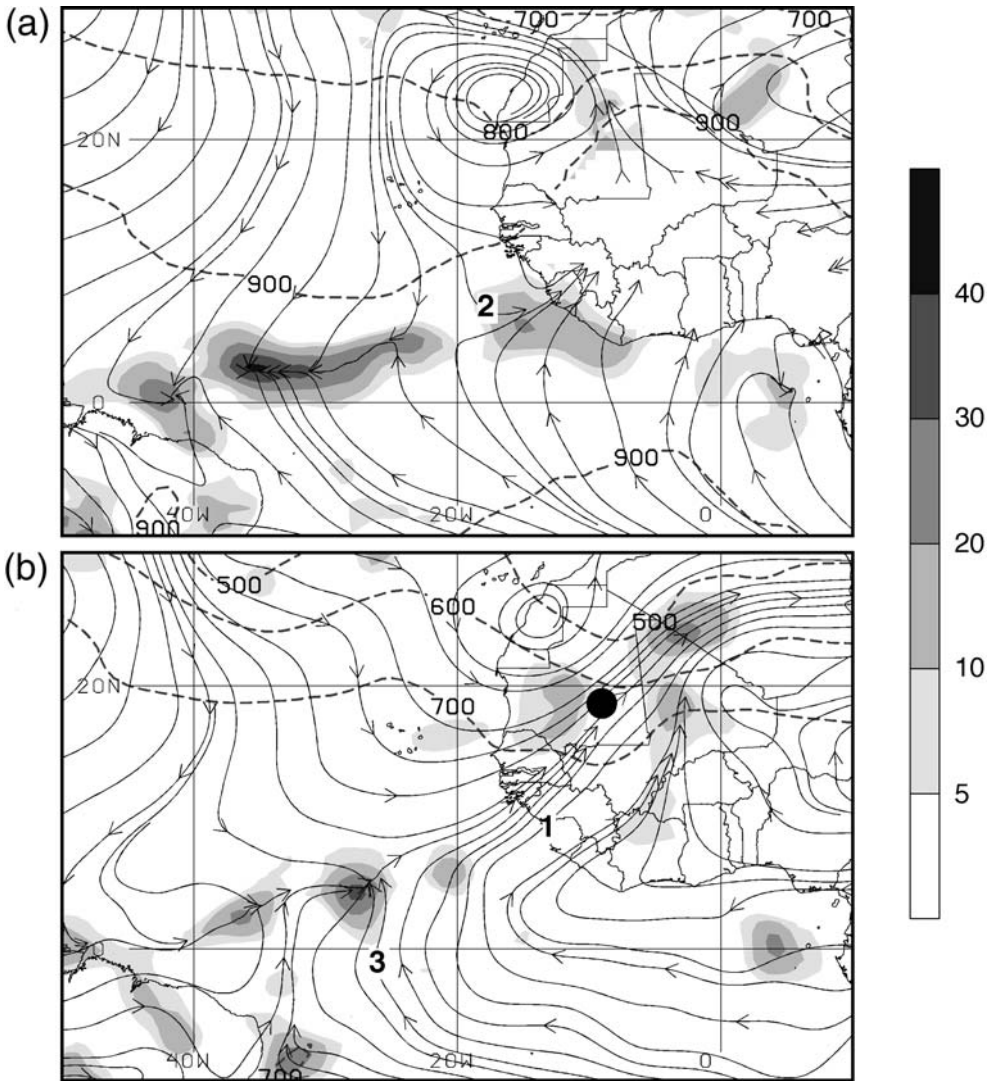


Figure 6. Case I at 12 UTC 7 January 2002 showing streamlines (full lines, arrowed), pressure (dashed lines at 100 hPa intervals) and convergence (shading according to key, in units of 10^{-6} s^{-1}) for isentropic surfaces: (a) 300 K, and (b) 310 K. The black dot in (b) marks the position of the vertical profile for 00 UTC 7 January shown in Fig. 11(c); bold numbers indicate the positions of the three trajectories from Fig. 5, each is shown at the level closest to the altitude of the trajectory.

(b) Case II

Figures 7 and 8 show the corresponding analyses for case II.

Trajectory 1 originates in the very moist (14.7 g kg^{-1}) near-surface ($\sim 900 \text{ m}$) south-westerly monsoon flow over West Africa (Figs. 7(a) and (d)). While moving northward the parcel warms and dries, presumably due to surface heat fluxes and mixing with continental air from farther north. By early 29 March the parcel has risen to 3.9 km, dried to 5.1 g kg^{-1} and increased its θ to 317 K. Remaining at altitudes around 4 km, the parcel flows adiabatically north-westward until it reaches Mauritania on 30 March.

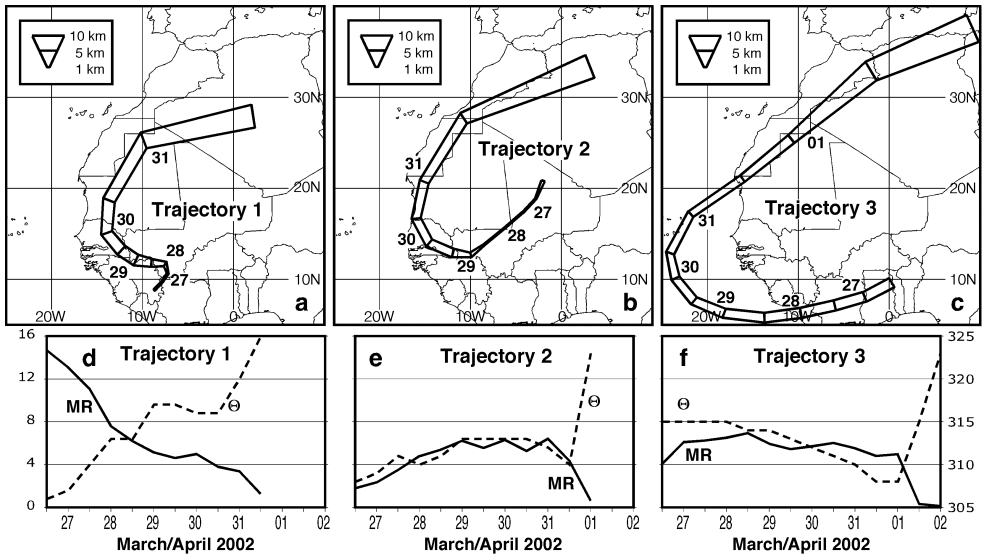


Figure 7. As Fig. 5 but for case II trajectories beginning at 15 UTC 26 March 2002.

The ensuing ascent to 7.4 km, coupled with warming and drying, suggests a contribution to the moderate rainfalls at the southern end of the precipitation zone (Fig. 1(b)).

Trajectory 2 starts in the extremely dry north-easterly trade flow over the Sahara, and remains at low-levels and close to the 310 K isentropic surface until it reaches its southernmost point early on 29 March (Figs. 7(b) and (e)). The steady moistening from 1.8 to over 6 g kg^{-1} during this period is possibly caused by its passage underneath a cloud band located over the Sahara between 26 and 28 March (not shown). FK03 noted observations of light rain at several hyper-arid stations in this region. On 29 March the parcel rises to over 3 km and warms to 313 K. Over the following 36 h only slight changes in height, MR and θ_e occur, while the trajectory curves anticyclonically into western Mauritania. On 31 March the parcel rises to 7.8 km and contributes to the rainfall over southern Morocco. Both trajectories 1 and 2 rise from near the surface to mid-levels at around $12\text{--}13^\circ\text{N}$ over West Africa. The latitudinal position and the depths of the vertical motion suggest a relation to the heat-low circulation at the intertropical discontinuity (ITD), which is part of the African monsoon system (Hastenrath 1985). Characterized by low-level confluence and convergence of monsoonal and Saharan air, large gradients of equivalent potential temperature, θ_e , and shallow rising motions, the ITD is evident in the model simulation at around 11°N everywhere on the West African continent and all through the day, but it is most pronounced at its western end and during the night. The latter agrees with observations (D. J. Parker, 2003, personal communication) and modelling studies (Racz and Smith 1999).

Trajectory 3 originates from the region of the weak mid-level African Easterly Jet (AEJ; Hastenrath 1985) and quickly propagates out to the Atlantic Ocean with only slight changes in height, MR and θ_e (Figs. 7(c) and (f)). Between 29 and 31 March the parcel sinks to 2.6 km, while curving anticyclonically towards Western Sahara. Reduction in both θ_e and MR suggest mixing with cooler and drier air. Subsequently rising to 9.3 km, the parcel contributes to the heavy rainfalls along the Moroccan–Algerian border around 00 UTC 1 April. Some qualitative agreement is found between trajectories 2 and 3, and the ECMWF trajectories shown in Fig. 6 of FK03.

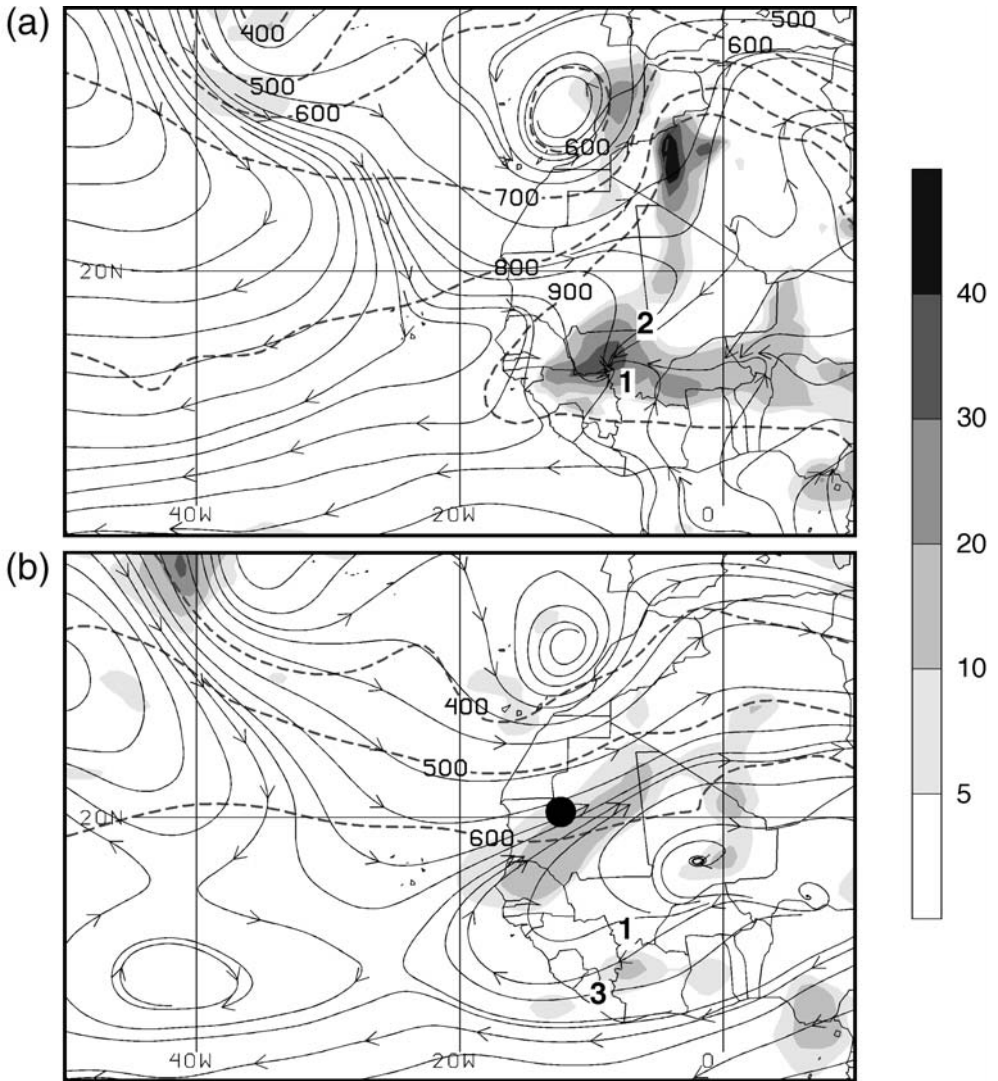


Figure 8. As Fig. 6 but for case II at 00 UTC 28 March 2002 at isentropic surfaces: (a) 305 K, and (b) 315 K. The black dot in (b) marks the position of the vertical profiles in Fig. 12(c). The bold numbers indicate the positions of the three trajectories from Fig. 7, each at the level closest to the respective altitude; however, as trajectory 1 is midway between the levels it is marked in both (a) and (b).

A low-level cyclonic circulation and north-westerly cold advection to the west of West Africa at 00 UTC 28 March are shown in Fig. 8. The associated trade surge at 305 K enhances the near-surface convergence at the western end of the ITD (Fig. 8(a)) and thereby supports the lifting of trajectories 1 and 2 to mid-levels. As in case I, the trade surge leads to an enhancement of near-equatorial convection, whose outflow feeds into the STJ accompanying the TP (KN05). At 315 K, parcels at the northern flank of the AEJ curve anticyclonically toward the low-pressure system to the north (Fig. 8(b)). Rising motion, warm advection and convergence characterize the region where this airstream meets the strong north-westerly flow from the Atlantic Ocean.

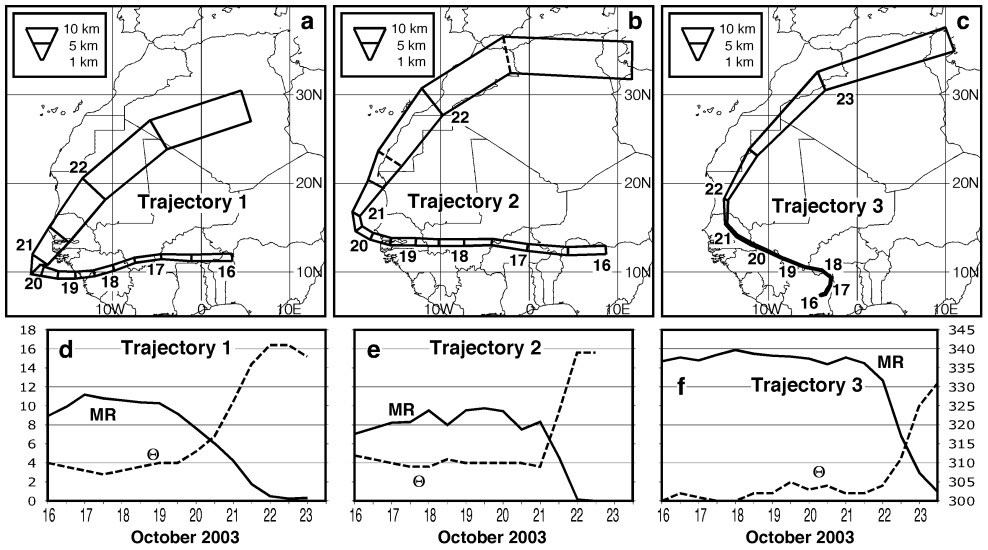


Figure 9. As Fig. 5 but for case III trajectories beginning at 00 UTC 16 October 2003.

(c) Case III

Figure 9 shows three example trajectories for case III.

Trajectories 1 and 2 both originate in the region of the AEJ over tropical Africa close to 12°N , and progress westward following the 310 K isentropic surface at 2–3 km. Note the northward displacement of the AEJ as compared to March/April (Fig. 7). Mixing ratios (MRs) vary between 7 and 11 g kg^{-1} with generally slightly higher values along the southern trajectory 1. On 20 October both trajectories turn north-eastward, and rise to well above 10 km in the following days. Showing the typical drying and warming, the trajectories contribute to the heavy rainfalls in Senegal and Mauritania on 21 October (trajectory 1), and Western Sahara and Morocco on 21/22 October (trajectory 2).

Trajectory 3 originates in the very moist low-level southerly monsoon flow over Africa (Figs. 9(c) and (f)). In contrast to trajectory 1 in Fig. 7, it remains in the lowest 1 km of the atmosphere while streaming north-westward into Senegal by 21 October. Throughout this period the parcel maintains its very high MR of $\sim 15\text{ g kg}^{-1}$ with θ just above 300 K. During 00 UTC 22 to 12 UTC 23 October the parcel rises from 1.7 to 8.1 km and releases nearly 12 g kg^{-1} of water into the heavy rainfalls over the north-western Sahara.

Figures 10(a) and (b) show the circulation at 300 and 310 K, respectively, at 00 UTC 20 October, when the AEJ trajectories in Fig. 9 turn northward towards the precipitation zone. Compared to the other cases, the cold advection and trade surge to the west of the trough are relatively weak. Instead, a low-level cyclonic centre is evident in the streamlines over south-western West Africa in connection with the strong convection depicted by the IR image in Fig. 4(a). It is the enhanced monsoonal flow to the north-east of this vortex that steers trajectory 3 towards the precipitation zone over Senegal. Strong trade wind flow from the SH appears to lend additional support to the northerly moisture transport (Fig. 10(a)). At 310 K the confluence between the extratropical north-westerly flow and the tropical easterlies steers trajectories 1 and 2 into the precipitation zone, in a similar (but weaker) fashion than in Figs. 6(b) and 8(b).

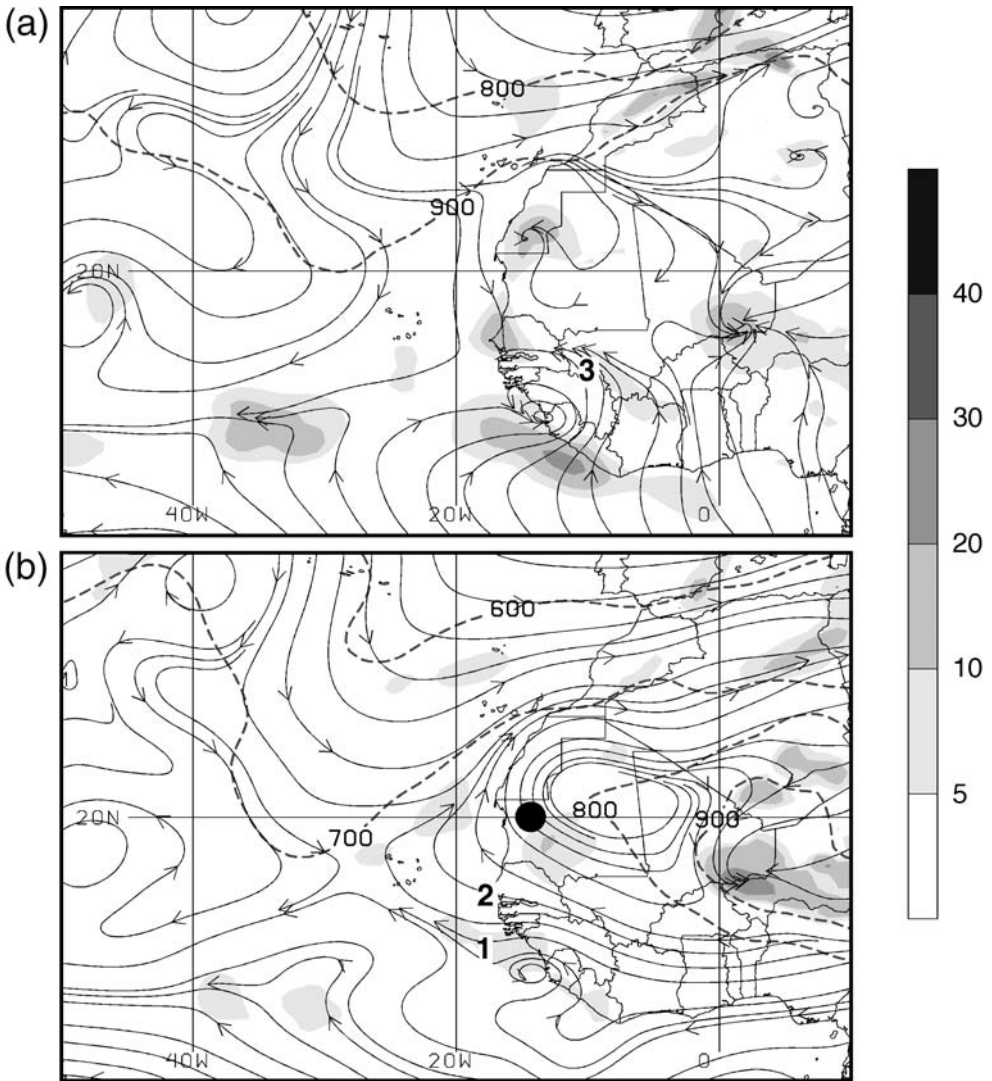


Figure 10. As in Fig. 6 but for case III at 00 UTC 20 October 2003. The black dot in (b) marks the position of the vertical profiles in Fig. 13(c). The bold numbers indicate the positions of the three trajectories from Fig. 9, each at the level closest to the altitude of the trajectory.

6. PRECIPITATION GENERATION

(a) Case I

During the 3 days preceding the rainfall event a short succession of two cyclonic disturbances to the west of West Africa is observed. As shown in the previous section, the first is involved in initiating the moisture transport from the Tropics (Fig. 6). After this disturbance has moved to the north-east and vanished (note the weak upper-trough over Morocco in Fig. 12(a)), a second trough takes its place (Fig. 2(b)). Figures 11(a) and (b) show the 500 hPa geopotential height distribution for these features at 00 UTC on 7 (trough 1) and 9 January (trough 2). We calculated the QG vertical velocity, ω , by solving the QG omega equation with a constant Coriolis parameter, f_0 , set equal

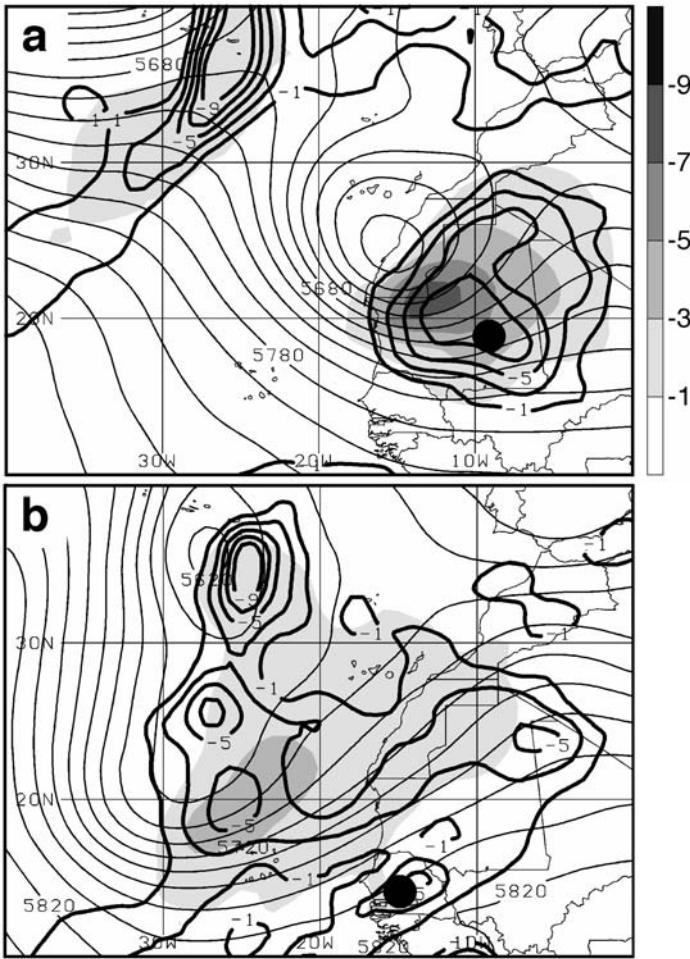


Figure 11. Case I: (a) 00 UTC 7 January 500 hPa geopotential height (thin lines, contour interval 20 gpm), vertical velocity w (thick lines, only negative values are given, contour interval $2 \times 10^{-1} \text{ Pa s}^{-1}$ starting at $-1 \times 10^{-1} \text{ Pa s}^{-1}$), and quasi-geostrophic vertical velocity ω (shading, contouring as for w); (b) as (a) but for 00 UTC 9 January 2002; (c) vertical profiles of relative humidity RH (solid lines), humidity mixing ratio MR (short dashes), and equivalent potential temperature θ_e (long dashes) for the times and locations indicated by the black dots in (a) (grey lines) and (b) (black lines). (d) For 00 UTC 9 January 2002 on the 345 K isentropic surface: streamlines, isotachs (dashed grey lines; m s^{-1}) and divergence (only positive values, shaded as key, 10^{-6} s^{-1}); thick black contours indicate regions of negative absolute geostrophic vorticity north of 15°N .

to the 25°N value. Input data are the model's geopotential height and temperature fields after a bi-linear interpolation to a $1^\circ \times 1^\circ$ latitude/longitude grid at 12 isobaric levels. The structure of ω displays little sensitivity to the choice of f_0 . Given that the Rossby number is on the order of 0.5 for the troughs shown in Fig. 11 (and in Figs. 12–13), results of the QG calculations have to be regarded with caution. They, nevertheless, convey quantitative estimates of how much of the model-generated uplift is related to temperature and vorticity advection by the upper-level troughs.

Figure 11(a) displays a closed low of 5592 gpm centred over the coast of Western Sahara with strong gradients on its western and southern flanks; ω reaches -0.8 Pa s^{-1} ($\sim 12 \text{ cm s}^{-1}$) to the south-east of the low and agrees well with vertical velocity, w , despite a slight shift of the maximum to the south-east. This gives support to

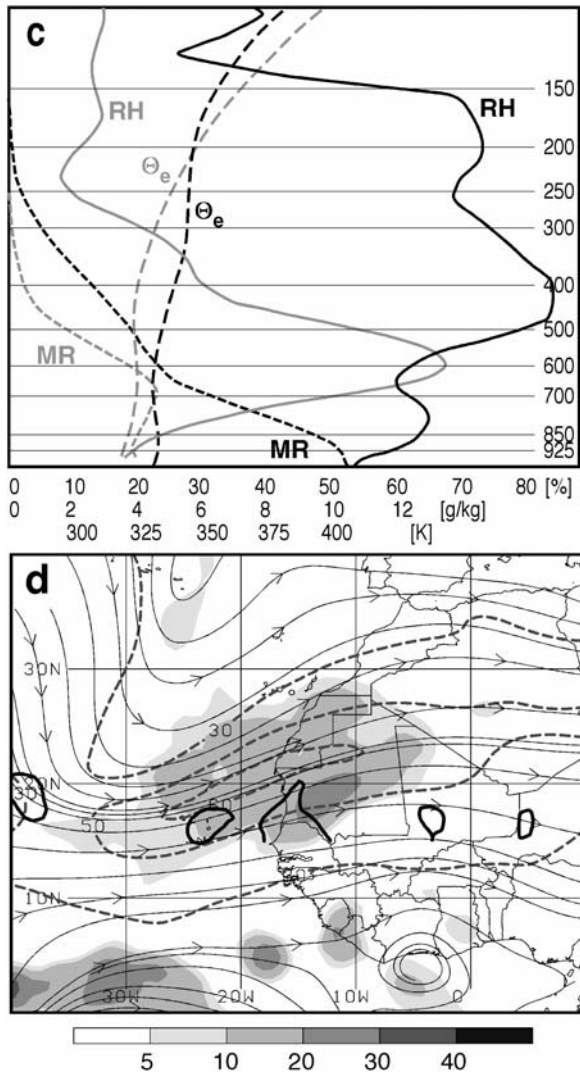


Figure 11. Continued.

the meaningfulness of QG diagnostics in this study. The dashed lines in Fig. 11(c) show vertical profiles of relative humidity, RH, MR, and θ_e at the location indicated by the filled circle in Fig. 11(a), which is characterized by considerable uplift and mid-level south-westerly flow from the Tropics (Fig. 6(b)). The latter leads to peaks in MR (~ 700 hPa) and in RH (~ 600 hPa) and a potential instability in the 650–450 hPa layer, as indicated by the decrease of θ_e with height. Despite the strong uplift, the air mass is too dry for this instability to be released. Consequently, only a subtropical cyclone-type cloud mass, a non-precipitating weak TP-like cloud band and a STJ streak of about 65 m s^{-1} formed in connection with trough 1 (not shown).

Compared to trough 1, trough 2 is more elongated, less deep (5647 gpm in its southern portion) and it is shifted to the south-west (Fig. 11(b)). The ω field is more

widespread and reaches only 55% of the maximum value associated with trough 1. Three different regions can be distinguished:

- Close to the trough axis two centres of strong uplift are found, where cloud condensation processes enhance the weak QG forcing (see Fig. 2(b)).
- In the cloud-free zone between the Canary Islands and about 15°N, 30°W (Fig. 2(b)) ω and w are in fairly good agreement.
- In the zone over West Africa that contains part of the TP, w is generally larger than ω .

Vertical profiles at the maximum in w over Senegal reveal that the moisture transports from the tropics (see subsection 5(a)) have led to substantially higher MRs throughout the troposphere (black lines in Fig. 11(c)). At lower levels the proximity to the coast certainly contributes to those differences. Since almost the entire troposphere is close to saturation (in particular 500–400 hPa), even weak forcing for uplift is sufficient to release the potential instability found at 850–650 hPa and eventually produce heavy precipitation (subsection 3(a)).

Figure 11(d) shows 345 K streamlines, isotachs and divergence for the same analysis time as in Figs. 2(b) and 11(b). Most of the divergence close to the axis of the upper-trough is consistent with the mid-level QG forcing shown in Fig. 11(b). Along the anticyclonic-shear side of the STJ, where parcels from very low latitudes accelerate north-eastward (Fig. 2(b)), areas of negative absolute geostrophic vorticity, η_g , indicate inertial instability (Holton 1992). The associated adjustment of mass and momentum supports the strong divergence and the ascent downstream over West Africa (cf. Uccellini *et al.* 1984). The convective outflow over Senegal around mid-day 9 January further increases the upper-level divergence, and therefore helps to sustain the instability and to spread the precipitation north-eastward. Surface cyclogenesis and frontogenesis under the upper-level subtropical cyclone (Fig. 2(b)) are weak throughout the development (not shown).

(b) Case II

Similar to developments in case I, a succession of two disturbances is observed within the 4 days before the precipitation event. While the first of these is responsible for the initiation of the moisture export from the Tropics (see subsection 5(b)), the second is directly associated with the rainfall over north-west Africa. Figures 12(a)–(c) show a comparison between the two troughs at 06 UTC on 27 and 30 March. Trough 1 appears as a closed 500 hPa low with a minimum height of 5566 gpm (Fig. 12(a)). The strong QG forcing of up to -0.74 Pa s^{-1} ($\sim 11 \text{ cm s}^{-1}$) to the east of the centre shows good structural agreement with w , but is slightly weaker. Vertical profiles of θ_e , RH and MR to the south-east of trough 1 reveal a layer of moist tropical air between 700 and 500 hPa (Fig. 12(c)), where south-westerly flow is observed at 00 UTC 28 March (Fig. 8(b)). This moist zone is surrounded by dry air below and aloft; the latter has presumably subsided within the cold trough to the north-west. RH values in the moist tongue are so small that the forcing for uplift is not sufficient to release the potential instability at 650–450 hPa, as indicated by the decrease of θ_e with height. Consequently the model does not generate any precipitation. As mentioned in subsection 5(b), the trough is, however, accompanied by a weak cloud band over the Sahara.

Trough 2 is comparably deep, but reveals a more wave-like elongated structure with a positive tilt (Fig. 12(b)). Whilst ω is slightly weaker than for trough 1, the forcing stretches farther into the Tropics. Over the Atlantic Ocean there is reasonable agreement between ω and w except for the regions where cloud condensation processes

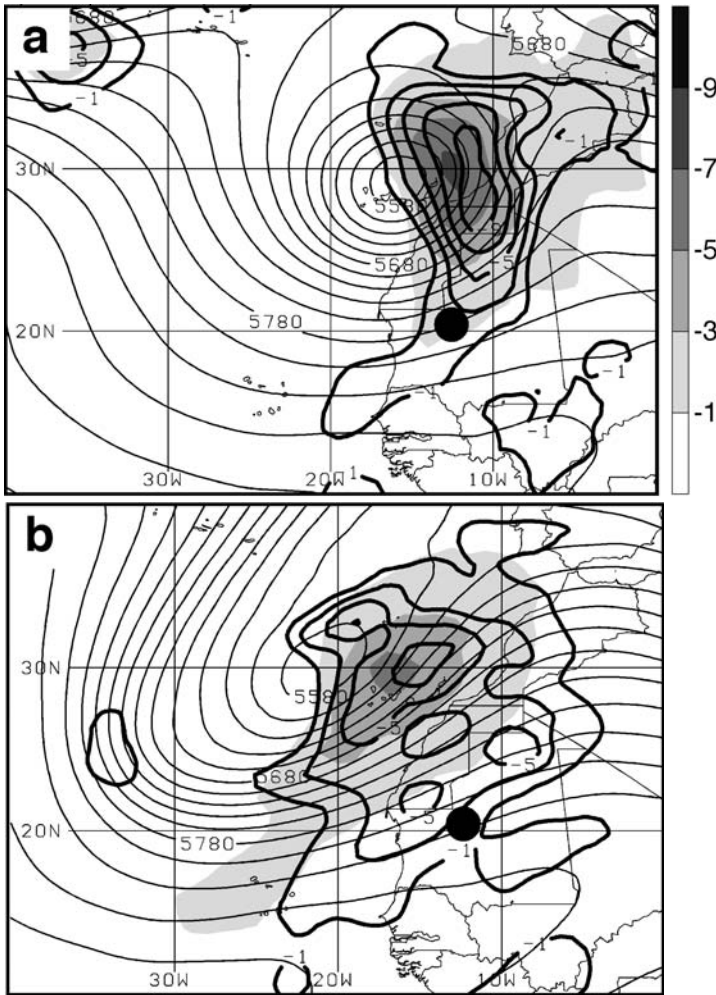


Figure 12. As Fig. 11 but for case II at 06 UTC 27 March 2002 ((a) and grey lines in (c)) and 06 UTC 30 March ((b), black lines in (c) and (d)).

near the subtropical cyclone enhance uplift. Over Africa w is substantially larger than ω . The vertical profiles at the same location as for trough 1 (black lines in Fig. 12(c)) reveal large increases in MR, RH and θ_e related to the export of moisture from the Tropics at lower levels (see subsection 5(b)) and to the TP at upper levels. Weak potential instability is found at mid-levels in agreement with a radiosonde ascent from Tindouf (see Table 1) at 12 UTC 30 March (FK03).

For 06 UTC 30 March, Fig. 12(d) shows that the region of strong uplift over Africa is characterized by pronounced 345 K divergence just downstream of an unusually large area of negative η_g along the anticyclonic shear side of the STJ (see also KN05). This suggests that the combination of weak QG forcing and inertial instability in an environment of weak stratification leads to the precipitation over north-western Africa, starting just a few hours later. At 07 UTC 1 April, w reaches a maximum of 23.5 cm s^{-1} at 30.3°N , 6.6°W , which compares well with ECMWF data (FK03). As in case I, surface cyclogenesis and frontogenesis underneath the upper-level subtropical cyclone (Fig. 3)

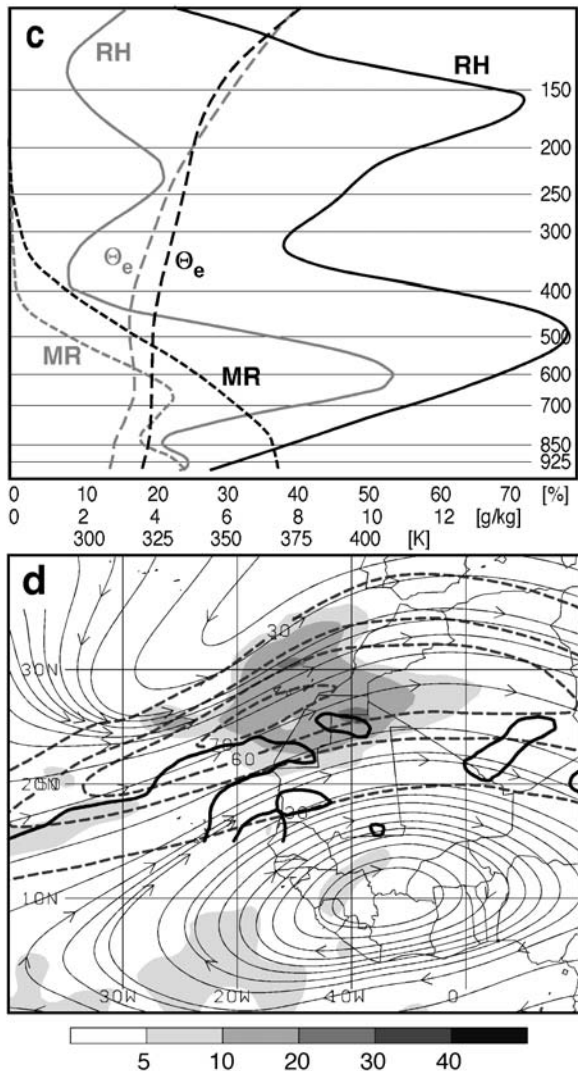


Figure 12. Continued.

are relatively weak (not shown). Only in the very late stages does a surface depression develop and move into the Mediterranean Sea (FK03).

(c) Case III

In contrast to cases I and II, only one significant disturbance is found to be responsible for both the moisture extraction from the Tropics (Fig. 10), and the precipitation and TP generation (Fig. 4) in case III. The 500 hPa geopotential height and vertical motion just before the beginning of the precipitation over Mauritania and two days earlier demonstrate the strong changes in circulation that occur with the arrival of the trough (Figs. 13(a) and (b)). QG forcing for uplift associated with this feature is widespread, but weak. To the west of Morocco a region of enhanced ascent is found

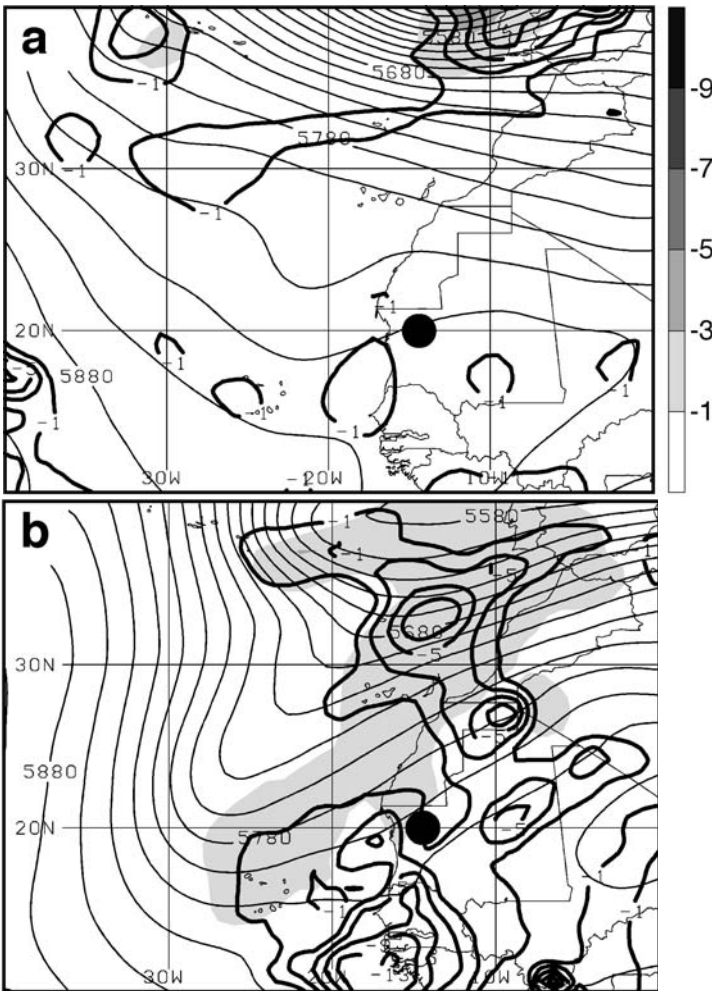


Figure 13. As Fig. 11 but for case III at 00 UTC 19 October 2003 ((a) and grey lines in (c)) and 00 UTC 21 October ((b), black lines in (c) and (d)).

that is most likely related to condensation within the clouds east of the trough axis (see Fig. 4).

Several areas of pronounced uplift are simulated over West Africa that are not strongly related to QG forcing. One is located to the south-west of Senegal and appears to be caused by tropical convection (Fig. 13(b)). Several processes are likely to have contributed to its intensification: dynamical forcing by the low-level wave (Fig. 10(b)); the trade wind surge over the Atlantic (Fig. 10(a)); and the inertial instability in the right-entrance region of the upper-jet (Fig. 13(d)) that facilitates the ventilation of outflow away from the convection (cf. Mecikalski and Tripoli 1998). While this highly divergent outflow (see Fig. 13(d)) leaves the deep tropics, it undergoes strong ageostrophic accelerations in order to achieve gradient wind balance. Entering the STJ to the east of the upper-level trough more ageostrophic accelerations ensue, which result in an explosively strengthening (see subsection 4(c)) upper-level jet. At 12 UTC 21 October, 12 h after the situation depicted in Fig. 13, ageostrophic wind speeds at 345 K reach

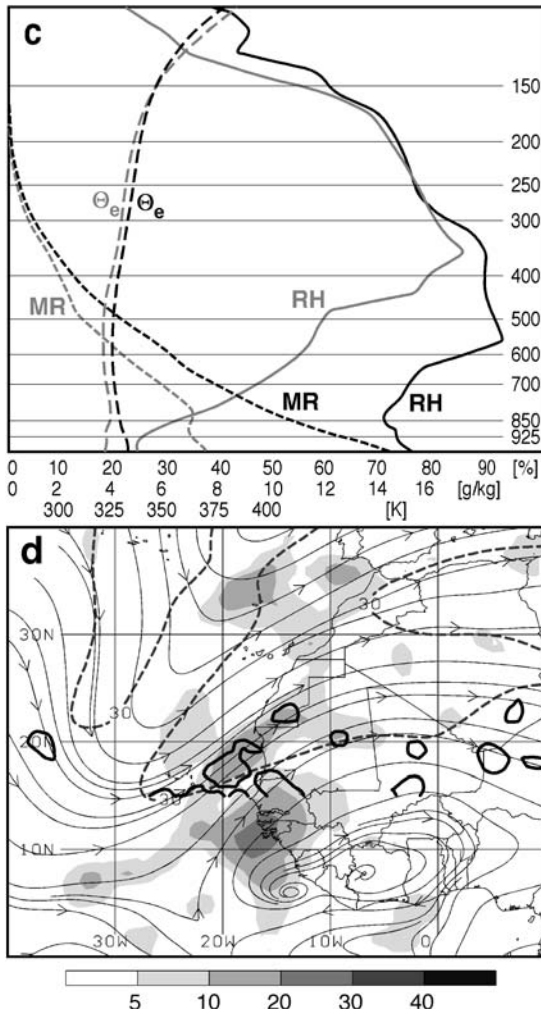


Figure 13. Continued.

45 m s^{-1} near the Cape Verde Islands ($\sim 18^\circ\text{N}$, 26°W ; not shown) where the total wind speed is only 28 m s^{-1} .

Figure 13(c) displays vertical profiles taken at 20°N , 14.5°W for the same analysis times as Figs. 13(a) and (b). They show a substantial increase in MR throughout the troposphere in connection with the moisture transports from the deep Tropics (see Fig. 10(b)), leading to near saturation between 500 and 600 hPa. Absolute moisture contents are higher than in the other two cases (note the different scales on the abscissa). Both profiles show signs of potential instability at lower levels, but only the high RH on 21 October allows a release of this instability. The forced ascent of this air mass through QG and inertial processes produces more divergent convective outflow, which in turn maintains the instability and allows precipitation to spread northwards into northwestern Africa along the southern flank of the jet axis. As in case II, it is only during the later stages of the development that surface cyclogenesis and low-level frontogenesis are involved in the generation of precipitation (not shown).

7. LARGE-SCALE ASPECTS

In this section we investigate the large-scale processes responsible for the penetration of the upper-level troughs into the subtropics and Tropics to the west of West Africa, with the help of maps of potential vorticity (PV) on the 335 K isentropic level (Hoskins *et al.* 1985). This level is located near the tropopause at midlatitudes (250–200 hPa) and extends down to below 400 hPa in the Tropics. At 12 UTC 4 January, two days before trough 1 of case I begins to affect West Africa, a strong PV gradient is found parallel to the east coast of North America (Fig. 14(a)). This region coincides with a strong upper-level jet of up to 92 m s^{-1} (not shown). Two surface cyclones form along the associated pronounced baroclinic zone at lower levels (black dots in Fig. 14). By 12 UTC 5 January the southern low-pressure system has remained close to the baroclinic zone and has intensified only marginally, but the northern low has deepened by 45 hPa to 944 hPa and has moved towards the southern tip of Greenland (Fig. 14(b)). This northern low fulfils the criteria for the ‘bomb’ classification by Sanders and Gyakum (1980), and ranks above the 99% percentile of the climatology by Roebber (1984).

The grey shading in Fig. 14 indicates the diabatic PV tendency in the 200–150 hPa layer using the method described in Cammas *et al.* (1994) and Posselt and Martin (2004). The explosive cyclogenesis is accompanied by strong frontogenesis, cloud-band formation and strong latent-heat release (not shown). This leads to a very intense reduction of upper-level PV which, together with the advection of low-PV air by the strong south-westerly winds, rapidly amplifies the PV ridge over the North Atlantic. This creates a large negative PV anomaly with values below 0.5 PVU^* as far north as 50°N (Fig. 14). The latter forces equatorward advection of high-PV air farther downstream, leading to the formation of trough 1 to the west of Africa. This process is accompanied by a distinct stratospheric intrusion, evident as a conspicuous dry swath in water vapour imagery behind the trough (not shown).

The large-scale evolutions leading to the generation of trough 2, as well as during case III, equally involve: a strong upper-level jet, frontogenesis, bomb-like cyclone deepening, cloud band formation, diabatic PV destruction and, finally, a distinct amplification of the PV wave over the North Atlantic (not shown). The generation of trough 1 in case II is in general agreement with these developments, but somewhat less dramatic. A fundamental difference is the additional contribution to the trough formation from the advection of high PV on the western side of an unusual bomb-like development over the subtropical Atlantic. Trough 2 of case II involves interactions with the STJ streaks over the southern US (see KN05) and a weak cyclogenetic but strongly frontogenetic development over North America.

The combination of the ageostrophic motions associated with the amplification of the extratropical PV wave with strong outflow both from the extratropical cloud band and from tropical convection, leads to massive upper-level convergence and widespread sinking over the subtropical Atlantic. The associated lower-level divergence is related to the enhancement of the trade winds over the eastern North Atlantic seen in Figs. 6, 8 and 10 (see also KN05 for case II).

These results reveal some interesting agreement with statistical investigations relating tropical convection/TP formation to the penetration of extratropical Rossby waves into the westerly duct regions (Webster and Holton 1982) in the tropical eastern Pacific and Atlantic (Liebmann and Hartmann 1984; Kiladis and Weickmann 1992, 1997; Iskenderian 1995; Kiladis 1998). Despite the smoothing introduced through filtering, averaging or compositing, these studies also find the influence of strong upstream

* $1 \text{ PVU} = 10^{-6} \text{ m}^2 \text{ s}^{-1} \text{ K kg}^{-1}$.

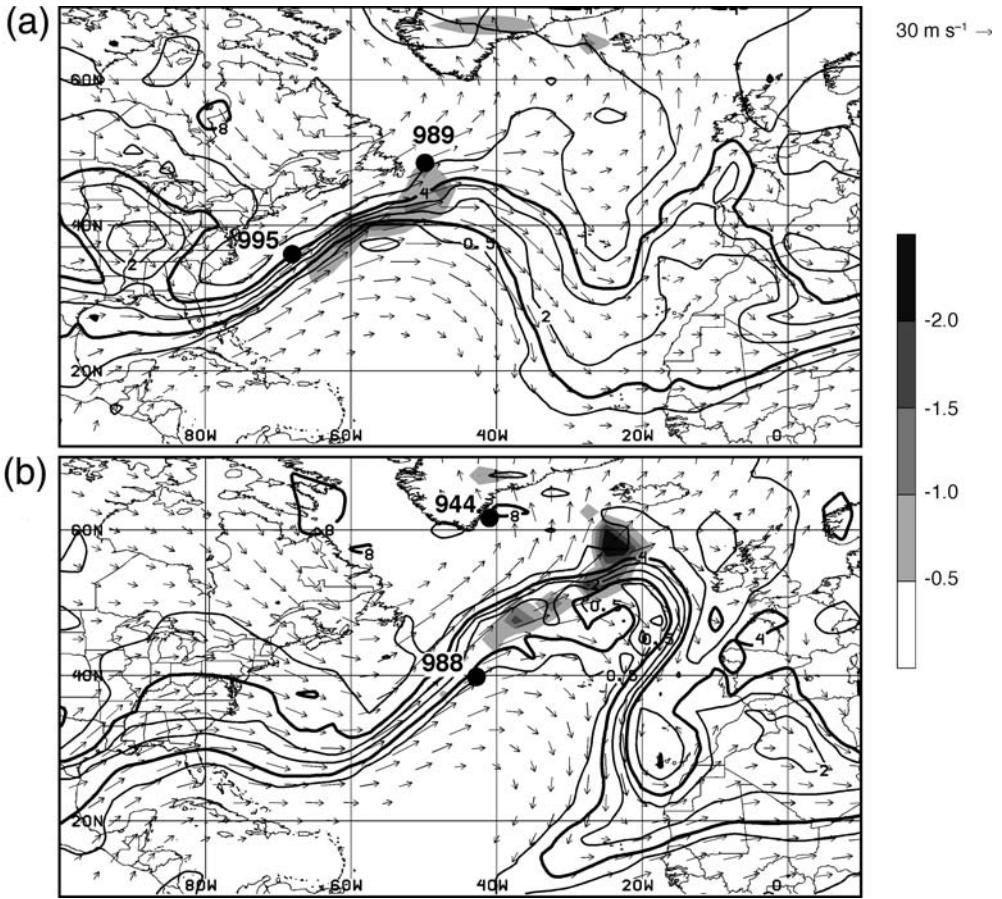


Figure 14. Case I: (a) 12 UTC 4 January, potential vorticity (PV; contours at 0.5, 1, 2, 3, 4, 6 and 8 PVU, the 1, 4 and 8 PVU contours are bold) and total wind vectors (scale in top right-hand corner, only winds greater than 15 m s^{-1} are plotted) on the 335 K isentropic surface, and diabatic PV tendency in the 150–200 hPa layer (shading as key, PVU day^{-1}). (b) As (a) but for 12 UTC 5 January 2002. Black dots indicate the positions and core pressures (in hPa) of selected surface cyclones as analysed on daily weather maps from the German Weather Service.

jets and ridges, trade surges, and upper-level convergence between outflow from tropical convection and an extratropical cloud band. It appears debatable, however, whether the waves can propagate into the Tropics, due to the existence of low-latitude westerlies (according to linear wave dispersion theory) or whether the diabatic and highly nonlinear interaction processes described here *force* the equatorward penetration of troughs, whose circulations produce the low-latitude westerlies.

8. SUMMARY AND CONCLUSIONS

This paper investigates the moisture transports and dynamics involved in three extended cool season cases of extreme rainfalls over subtropical and tropical West Africa, using observational data and output from a simulation by the UW-NMS. Satisfactory agreement is found between the model data and rain-gauge measurements, which points to a large-scale control of the rainfalls and a substantial degree of predictability, especially in comparison to tropical convection. An upper-level trough to the west of West

Africa, a strong STJ streak and a TP are characteristic of all three cases. Cases I and III revealed rather explosive cloud and jet developments, almost south–north oriented TP axes, and a strong relation to the tropical convection at the southern end of the TP. Nevertheless their evolution basically agrees with the concept of TP genesis proposed by KN05 based upon a detailed study of case II.

As revealed by trajectory analysis, the generation of precipitation involved the transport of moisture from three source regions in the Tropics: (i) the mid-level tropical easterlies; (ii) the near-surface north-easterly trade winds over the Sahara, after moistening through fluxes from the ocean (case I) or through precipitation from a prior cloud band (case II); and (iii) the moist southerly monsoon flow over Africa (cases II and III). The air parcels whose trajectories were followed in (ii) and (iii) were eventually lifted to mid-levels in the region of the ITD. Finally parcels from all three source regions dropped all their moisture over the precipitation zones in West Africa accompanied by strong ascent. Outgoing long-wave radiation data (not shown) indicate active westward moving equatorial Rossby waves (cf. Fig. 3 in Kiladis 1998) that may have further supported the export of moisture.

During cases I and II the rainfall events involved a short succession of two cyclonic disturbances. The first disturbance was instrumental for extracting tropical moisture and steering it into the circulation of the second disturbance, which was then dynamically involved in the precipitation generation. Since the vertical motions associated with the initial disturbance mainly affected dry subtropical air masses, they generated little or no precipitation. This is typical of maritime subtropical cyclones, which often remain upper-level features with weak cloud developments. In case III, which was in October when the deep layer of moisture associated with the African monsoon is in a more northerly position, no significant prior disturbance was involved and the northward transport of moisture appeared to be supported by strong trade winds from the SH and a low-level tropical vortex. This situation is in qualitative agreement with the idea of Soudano–Saharan depressions resulting from an interaction between low-level African easterly waves and troughs in the upper-level westerlies (see Fig. 3 in Nicholson 1981).

In all three cases the mid-level moisture transports produced a potentially unstable stratification. Especially during cases I and II, the shielding of solar radiation by the TP clouds well before the rain began (e.g. Fig. 2(b)) suggests a minor role for surface heating in generating vertical instability, in contrast to summer cases (Knippertz *et al.* 2003b). Given the high RH in the tropical air, the release of this instability was achieved through weak QG forcing at the south-eastern fringe of the upper-level trough, and strong upper-level ageostrophic winds caused by the inability of the atmosphere to balance the outflow from tropical convection in the environment of a strong baroclinic jet (see KN05). The impact of inertial instability along the anticyclonic shear side of the jet on upper-level divergence and uplift is an important extension to the work of Ziv (2001), who considered positive vorticity advection at the inflection point of the merged polar and STJs as the main factor. This analysis is consistent with the observation by Knippertz (2004) that precipitation in southern Morocco often occurs far to the east of the upper-trough axis. FK03 speculate that orographic lifting contributed to the precipitation generation during case II but, at least in the model, heaviest precipitation fell in the less elevated region along the Moroccan–Algerian border (Fig. 1(b)). Weak cyclogenesis and frontogenesis was observed only at the late stages of the development (cf. Thepenier and Cruette 1981).

Despite the different seasons and geographical locations of the extreme precipitation, the three cases reveal similarities in the large-scale upstream flow. The upper-level troughs examined took the form of positively tilted, elongated PV streamers that

formed through an equatorward transport of high values of PV downstream of a high-amplitude ridge, consistent with the LC1 life cycle of baroclinic waves described by Thorncroft *et al.* (1993). The rapid amplification of the ridges was achieved through negative PV advection and diabatic PV reduction due to strong latent heating within an upstream cloud band (see Stoelinga 1996; Massacand *et al.* 2001). The latter was connected to explosive cyclogenesis near the east coast of North America, where rapid deepening is promoted by the strong land–sea temperature contrast during the winter half year (Sanders and Gyakum 1980; Roebber 1984). The amplifying extratropical PV waves and outflow from tropical convection generated strong upper-level convergence, sinking and low-level divergence to the west of the troughs penetrating to low latitudes. The resulting north-westerly cold advection enhanced the trade winds (trade surge), the uplift along the ITD over Africa, and near-equatorial low-level convergence and convection over the tropical Atlantic, leading to a subsequent acceleration of the downstream STJ. In the case of repeated extratropical forcing by two troughs a positive feedback on the local Hadley overturning is observed (see KN05).

The present study demonstrates that tropical moisture transports and upper-level dynamical forcing are crucial ingredients for TP formation and heavy precipitation. Thus a possible reason why northern hemisphere TPs (Kuhnel 1989; Iskenderian 1995) and tropically related precipitation in north-west Africa (Knippertz 2003) are most common during the transition seasons is the coexistence of strong baroclinic developments and a relatively northerly position of tropical moisture, one of which is absent in the peak seasons. Knippertz *et al.* (2003b) support this by showing that occasional outbreaks of tropical moisture in summer only result in light localized precipitation, where the heating of elevated terrain compensates for the lack of dynamical forcing. Future work should investigate more cases of equatorward penetrations of extratropical troughs and major TP-related precipitation events, in order to better understand and to compare the processes affecting different regions and seasons. It would also be interesting to study the impacts of a suppression of latent heating on the large-scale evolution in model simulations (Stoelinga 1996; Massacand *et al.* 2001). It seems noteworthy that the present cases are embedded in periods of strong hemispheric TP activity (e.g. January 2002). Therefore more statistical approaches should be used in the long run to quantify the contribution of tropical–extratropical interactions to the hemispheric circulation, as well as to extreme and climatological rainfall in the subtropics and Tropics.

ACKNOWLEDGEMENTS

The scientific results presented in this paper were accomplished during a 2 year postdoctoral research scholarship from the German Science Foundation (DFG; Grant KN 581/1–1) at the Department of Atmospheric and Oceanic Sciences of the University of Wisconsin–Madison under the supervision of Professor Jonathan E. Martin and Professor emeritus Stefan L. Hastenrath. We would like to thank Dr John R. Mecikalski for his help with running the UW-NMS model, Peter Pokrandt for his assistance in data and software issues, and two anonymous reviewers for their helpful comments on an earlier version of the manuscript. We are grateful for the high-resolution precipitation data provided by the IMPETUS project.

REFERENCES

- Camberlin, P. and Diop, M. 2003 Application of daily rainfall principal component analysis to the assessment of the rainy season characteristics in Senegal. *Clim. Res.*, **23**, 159–169

- Cammas, J.-P., Keyser, D., Lackmann, G. M. and Molinari, J. 1994 'Diabatic redistribution of potential vorticity accompanying the development of an outflow jet within a strong extratropical cyclone'. Pp. 403–409 in Preprints of the international symposium on the life cycles of extratropical cyclones, Vol. II. Bergen. Geophysical Institute, University of Bergen, Norway
- Dayan, U. and Abramski, R. 1983 Heavy rain in the Middle East related to unusual jet stream properties. *Bull. Am. Meteorol. Soc.*, **64**, 1138–1140
- FAO 2004 *Desert locust bulletin, No. 303*. Food and Agriculture Organization of the United Nations, Rome, Italy
- Fink, A. H. and Knippertz, P. 2003 An extreme precipitation event in southern Morocco in spring 2002 and some hydrological implications. *Weather*, **58**, 377–387
- Griffiths, J. F. and Soliman, K. H. 1972 The northern desert (Sahara). Pp. 75–132 in *World survey of climatology*. Ed. H. E. Landsberg. *Climates of Africa*, Volume 10, Elsevier, New York, USA
- Hastenrath, S. 1985 *Climatic and circulation of the Tropics*. D. Reidel Publishing Company, Dordrecht, the Netherlands
- Hibbard, W., Anderson, J., Foster, I., Paul, B., Jacob, R., Schafer, C. and Tyree, M. 1996 Exploring coupled atmosphere–ocean models using Vis5D. *Int. J. Supercomputer Appl.*, **10**, 211–222
- Holton, J. R. 1992 *An introduction to dynamic meteorology*. Third edition. Academic Press, New York, USA
- Hoskins, B. J., McIntyre, M. E. and Robertson, A. W. 1985 On the use and significance of isentropic potential vorticity maps. *Q. J. R. Meteorol. Soc.*, **111**, 877–946
- Iskenderian, H. 1995 A 10-year climatology of northern hemisphere tropical cloud plumes and their composite flow patterns. *J. Climate*, **8**, 1630–1637
- Kiladis, G. N. 1998 Observations of Rossby waves linked to convection over the eastern tropical Pacific. *J. Atmos. Sci.*, **55**, 321–339
- Kiladis, G. N. and Weickmann, K. M. 1992 Extratropical forcing of tropical Pacific convection during northern winter. *Mon. Weather Rev.*, **120**, 1924–1938
- 1997 Horizontal structure and seasonality of large-scale circulations associated with submonthly tropical convection. *Mon. Weather Rev.*, **125**, 1997–2013
- Knippertz, P. 2003 Tropical–extratropical interactions causing precipitation in northwest Africa: Statistical analysis and seasonal variations. *Mon. Weather Rev.*, **131**, 3069–3076
- 2004 A simple identification scheme for upper-level troughs and its application to winter precipitation variability in northwest Africa. *J. Climate*, **17**, 1411–1418
- 2005 Tropical–extratropical interactions associated with an Atlantic tropical plume and subtropical jet streak. *Mon. Weather Rev.*, in press
- Knippertz, P., Christoph M. and Speth, P. 2003a Long-term precipitation variability in Morocco and the link to the large-scale circulation in recent and future climates. *Meteorol. Atmos. Phys.*, **83**, 67–88
- Knippertz, P., Fink, A. H., Reiner, A. and Speth, P. 2003b Three late summer/early autumn cases of tropical–extratropical interactions causing precipitation in northwest Africa. *Mon. Weather Rev.*, **131**, 116–135
- Kuhnel, I. 1989 Tropical–extratropical cloudband climatology based on satellite data. *Int. J. Climatol.*, **9**, 441–463
- Liebmann, B. and Hartmann, D. L. 1984 An observational study of tropical–midlatitude interaction on intraseasonal time scales during winter. *J. Atmos. Sci.*, **41**, 3333–3350
- McGuirk, J. P., Thompson, A. H. and Schaefer, J. R. 1988 An Eastern Pacific tropical plume. *Mon. Weather Rev.*, **116**, 2505–2521
- Massacand, A. C., Wernli, H. and Davies, H. C. 2001 Influence of upstream diabatic heating upon an Alpine event of heavy precipitation. *Mon. Weather Rev.*, **129**, 2822–2828
- Mecikalski, J. R. and Tripoli, G. J. 1998 Inertial available kinetic energy and the dynamics of tropical plume formation. *Mon. Weather Rev.*, **126**, 2200–2216
- 2003 Influence of upper-tropospheric inertial stability on the convective transport of momentum. *Q. J. R. Meteorol. Soc.*, **129**, 1537–1563
- Nicholson, S. E. 1981 Rainfall and atmospheric circulation during drought periods and wetter years in West Africa. *Mon. Weather Rev.*, **109**, 2191–2208

- Nicholson, S. E. 2001 Climate and environmental change in Africa during the last two centuries. *Clim. Res.*, **17**, 123–144
- Posselt, D. J. and Martin, J. E. 2004 The effect of latent heat release on the evolution of a warm occluded thermal structure. *Mon. Weather Rev.*, **132**, 578–599
- Racz, Z. and Smith, R. K. 1999 The dynamics of heat lows. *Q. J. R. Meteorol. Soc.*, **125**, 225–252
- Ramage, C. S. 1962 The subtropical cyclone. *J. Geophys. Res.*, **67**, 1401–1411
- Roebber, P. J. 1984 Statistical analysis and updated climatology of explosive cyclogenesis. *Mon. Weather Rev.*, **112**, 1577–1589
- Sanders, F. and Gyakum, J. R. 1980 Synoptic–dynamic climatology of the ‘bomb’. *Mon. Weather Rev.*, **108**, 1589–1606
- Stoelinga, M. T. 1996 A potential–vorticity-based study of the role of diabatic heating and friction in a numerically simulated baroclinic cyclone. *Mon. Weather Rev.*, **124**, 849–874
- Thepenier, R.-M. and Cruette, D. 1981 Formation of cloud bands associated with the American subtropical jet stream and their interaction with midlatitude synoptic disturbances reaching Europe. *Mon. Weather Rev.*, **109**, 2209–2220
- Thorncroft, C. D., Hoskins, B. J. and McIntyre, M. E. 1993 Two paradigms of baroclinic-wave life-cycle behaviour. *Q. J. R. Meteorol. Soc.*, **119**, 17–55
- Trenberth, K. E. 1992 ‘Global analyses from ECMWF and atlas of 1000 to 10 mb circulation statistics’. NCAR Tech Note, NCAR/TN-373+STR NTIS PB92-218718/AS. National Center for Atmospheric Research, Boulder, CO, USA
- Tripoli, G. J. 1992 A nonhydrostatic numerical model designed to simulate scale interaction. *Mon. Weather Rev.*, **120**, 1342–1359
- Uccellini, L. W., Kocin, P. J., Petersen, R. A., Wash C. H. and Brill, K. F. 1984 The Presidents’ Day cyclone of 18–19 February 1979: Synoptic overview and analysis of the subtropical jet streak influencing the pre-cyclogenesis period. *Mon. Weather Rev.*, **112**, 31–55
- WMO 1996 ‘Climatological normals (CLINO) for the period 1961–90’. WMO-No. 847. World Meteorological Organization, Geneva, Switzerland
- Webster, P. J. and Holton, J. R. 1982 Cross-equatorial response to middle-latitude forcing in a zonally varying basic state. *J. Atmos. Sci.*, **39**, 722–733
- Wright, W. J. 1997 Tropical–extratropical cloudbands and Australian rainfall: I. Climatology. *Int. J. Climatol.*, **17**, 807–829
- Ziv, B. 2001 A subtropical rainstorm associated with a tropical plume over Africa and the Middle-East. *Theor. Appl. Climatol.*, **69**, 91–102